Progress In Electromagnetics Research M, Vol. 117, 119–128, 2023

A Circular Split Ring Resonator Absorber with Graphene Material for Terahertz Communication Applications

Nagandla Prasad[1], Pokkunuri Pardhasaradhi[1], Boddapati T. P. Madhav[1, *], Yarlagadda Ramakrishna[2], and Yepuri A. Hasitha[3]

Abstract—In this research article, we propose a split ring resonator (SRR) based metasurface absorber based on graphene material. The performance of the graphene-based absorber at terahertz frequencies can be altered by varying the chemical potential of graphene material. Because of its excellent tunability and optical responsiveness at terahertz frequency, graphene-based metamaterials have been widely used in optoelectronic devices, sensors, filters, and many more. The proposed structure contains three layers namely graphene-based patch as a conductive layer, lossy silicon as a dielectric layer, and finally gold as a bottom conductive layer. The proposed unit cell resonates at three different absorption peak frequencies of 2.91 THz, 8.1 THz, and 9.61 THz with operating frequency bands at (2.66 THz to 3.12 THz), (7.71 THz–8.47 THz), and (9.57 THz–9.63 THz), respectively. The purpose of this research is to present a thorough investigation of graphene-based THz metamaterial absorbers, including modeling and verification of the structure through an equivalent circuit approach. It is very much beneficial to understand the conductive phenomenon of graphene material by tuning the Fermi chemical potential and achieve a high percent level of absorption for the corresponding absorption frequency bands.

1. INTRODUCTION

Researchers from all over the world are paying more attention towards the terahertz communication, which has a frequency range of 0.1 THz to 10 THz [1], and its wavelength range is from 30 micrometers to 3 millimeters. As terahertz frequency range contains high speed and larger bandwidth, it can be used for various applications like detecting faults in tablet coating through product inspection, chemical [2], astronomical [3], and physics applications like material characterization [4], medical applications like cancer detection [5], security applications like detecting weapons in the airports [6], military applications [7], 6G applications [8], sensing applications [9], and many more. Over the last few decades, metamaterial based structures for terahertz frequency domain have attracted a great deal of interest. The reason for this interest is a lack of natural materials with a strong reactivity to terahertz electromagnetic (EM) radiation. Metamaterials are artificially created structures that exhibit amazing and distinct properties that natural materials do not have. Generally, the permittivity and permeability qualities are used to identify the metamaterial based structures. There is a lot of scope to produce a high bandwidth and high percent level of absorbers by incorporating graphene material to the metasurface's radiating patch. Graphene is a more flexible material with higher electronic conductivity than copper or other conductive materials. Not only is graphene thin, but it is also extremely transparent to visible light. Because of its excellent physical features, such as surface plasmon resonance, ultrafast response speed, high bandwidth, ultrahigh carrier mobility, and tuneability, graphene has been extensively

Received 21 April 2023, Accepted 10 June 2023, Scheduled 20 June 2023

* Corresponding author: Boddapati Taraka Phani Madhav (btpmadhav@kluniversity.in).

[1] Antennas and Liquid Crystals Research Center, Department of ECE, Koneru Lakshmaiah Education Foundation, Vaddeswaram, Guntur, Andhra Pradesh, India. [2] Seshadri Rao Gudlavalleru Engineering College, Gudlavalleru, AP, India. [3] Department of CSE, Vellore Institute of Technology, AP, India.

explored as a revolutionary material over the last few years. It is substantially strong compared to other materials and contains a nano thickness.

Zhou et al. [10] suggested a dual-band metasurface absorber using a simple circle-shaped graphene material as a radiating conductive patch with an overall unit cell size in two dimensions and obtained a maximum absorption percentage of 98.2%. By employing graphene's tunability capability, Li et al. [11] presented broadband and narrow-band absorptivity levels inside the same structure. Zhang et al. [12] proposed a graphene-based absorber with optical bi-stability with a low threshold and large extinction ratio in the near-IR band. Upender and Kumar [13] proposed a graphene-based circular ring-shaped metasurface absorber for biosensing applications. Beheshti Asl et al. [14] proposed a multilayered graphene-based construction to increase the absorption bandwidth and level of the metasurface absorber. To achieve the optical performance, Yi et al. [15] presented a metasurface absorber based on a square-square-circle graphene array. Ashvanth et al. [16] provided another graphene-based adjustable metasurface absorber by altering the chemical potential, and the suggested tunable absorber comprises six V-shaped stubs with graphene material at the corners to generate six absorption bands. Xu et al. [17] proposed a polarization-insensitive and incidence angle-insensitive nature with a complementary graphene material-based T-shaped structure for generating dual bands and three absorption bands by adjusting graphene chemical potential. Jain et al. [18] reported a graphene metasurface-based polarization-insensitive quadband absorber for terahertz applications.

In this proposed work, we finalize three split-ring resonators after performing some parametric analysis for the proposed work. The structure operates at three resonant frequency bands and produces a high percent level of absorption. It is a straightforward structure with three layers with a compact size. Finally, it produces polarization-insensitive capability, which reveals the structure performance for any polarization angle. A better performance can be achieved by varying the chemical potential of graphene material.

2. GRAPHENE CONDUCTIVITY PHENOMENON

Exfoliation, chemical vapour deposition (CVD), thermal exfoliation, and carbon separation are the steps used to obtain a graphene sheet or layer from graphite bulk material. At higher frequencies, graphene material shows surface plasmon resonance (SPR), higher mobility, and environmental resilience. As a result, graphene is an ideal material for terahertz applications. The graphene material influences graphene conductivity and other properties including mobility of an electron, temperature, relaxation time, Fermi level, and frequency. In general, surface conductivity is utilized to express graphene's behavior. Li and Yu [21] proposes that the surface conductivity of graphene material has intra- and inter-bands, which are represented by the following formulae [21–23].

$$\sigma_g = N_g \times (\sigma_{\text{inter}} + \sigma_{\text{intra}}) \tag{1}$$

$$\sigma_{\text{inter}} = \frac{ie^2}{4\Pi\hbar^2} \ln\left[\frac{2\,|\mu_c| - (\omega + 2i\Gamma)\hbar}{2\,|\mu_c| + (\omega + 2i\Gamma)\hbar}\right] \tag{2}$$

$$\sigma_{\text{intra}} = \frac{ie^2 k_B T}{\Pi\hbar^2(\omega + 2i\Gamma)} \left[\frac{\mu_c}{k_B T} + 2\ln\left(1 + \exp\left(\frac{\mu_c}{k_B T}\right)\right)\right] \tag{3}$$

Since

$$|\mu_c| \gg k_B T \tag{4}$$

the inter part of Equation (1) is ignored, so the equation will become as following 5^{th} equation

$$\sigma_g = \frac{ie^2\mu_c}{\Pi\hbar^2(\omega + 2i\Gamma)} \tag{5}$$

$$\hbar \times 2\Pi = h \tag{6}$$

$$\tau = \frac{v\mu_c}{eV_F^2} \tag{7}$$

$$\Gamma = \frac{1}{2\tau} \tag{8}$$

$$V_g = \frac{q\mu_c^2 h}{\Pi\hbar^2 V_F^2 \varepsilon_0 \varepsilon_r} \tag{9}$$

where N_g is the number of graphene layers, $e = 1.6 \cdot 10^{-19}$ C the charge of an electron, ω the angular frequency, τ the relaxation time, k_B the Boltzmann constant, $\hbar$ the reduced plank constant, μ_c the graphene chemical potential, and T the absolute temperature in Kelvin. The conductivity due to inter band can be discarded for infrared and terahertz ranges. $V_F = 9.5 \times 10^5$ m/s$\simeq 10^6$ m/s indicates Fermi velocity, and Γ is the scattering rate.

3. STRUCTURE DESIGN

Transmission line theory may be utilized to illustrate the idea of EM wave absorption. To accomplish good EM wave absorption, the metamaterial impedance must match the EM wave impedance to the metasurface. To determine the absorption of a metasurface, use the formula below. In general, the absorption of a metasurface absorber may be expressed in terms of S-parameters as follows.

$$\text{Absorption}\,(A) = 1 - abs\left(S_{11}^2\right) - abs\left(S_{21}^2\right) \tag{10}$$

From the equation, we can say that A represents the absorption, $|S_{11}^2|$ the reflection coefficient, and $abs(S_{21}^2)$ the transmission coefficient of an absorber. Because the bottom layer of the proposed absorber is a perfect conducting material like gold, the transmission coefficient is almost zero (i.e., $abs(S_{21}^2) = 0$) for the metasurface absorber. Equation (1) can be reformulated as follows.

$$\text{Absorption}\,(A) = 1 - abs\left(S_{11}^2\right) \tag{11}$$

The proposed structure contains three layers namely gold as a bottom reflector, silicon as a dielectric layer, and graphene as a radiating patch. The dimensions of the proposed structure are clearly indicated in Table 1. As shown in Figure 1, the radiating patch of the proposed unit cell contains a square-typed ring and two circular typed SRRs. The outer SRR is attached to the square typed ring with a strip width (w) of 0.5 micrometers. The outer and inner split gaps are indicated by g, and both contain the same size of 0.5 micrometers. The magenta color indicated in the structure represents lossy silicon material containing a dielectric constant of 11.9. Finally, a gold material-based reflector is placed at the bottom of the structure to stop the EM wave transmission. So only reflection and absorption take place for Figure 1. For designing the proposed unit cell, CSTMW studio-2020 numerical simulation tool was utilized. During the simulation process, a frequency range is specified in the simulation setup, and then perfect electric and magnetic boundary conditions are applied along x and y axes, to impinge the EM wave along the z-direction.

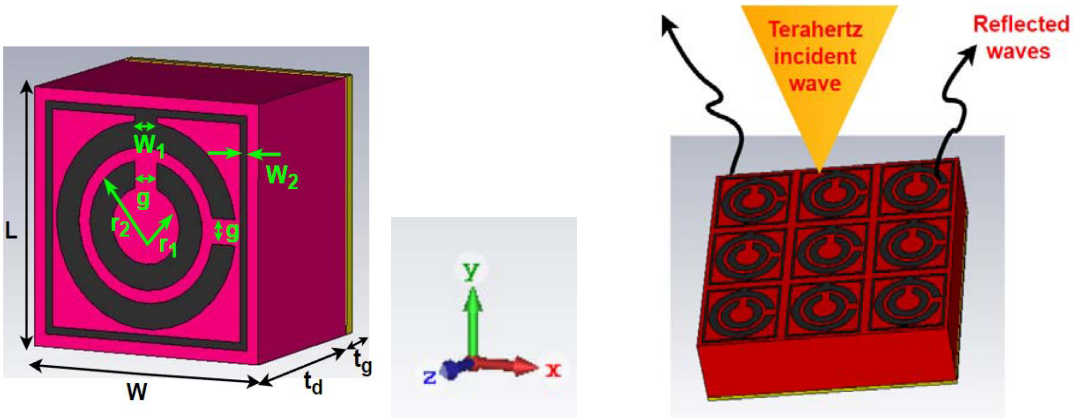

(a) (b)

Figure 1. Proposed (a) unit cell structure with dimensions (All are in micrometers), (b) absorber.

Table 1. Proposed structure dimensions.

Parameter	L	W	W_1	W_2	g	r_1	r_2	t_d	t_g
Dimension (micrometers)	10	10	0.5	0.3	0.5	1.5	3	9	0.5

4. RESULTS AND DISCUSSION

The conductivity of graphene material can be varied, and better performance is achieved by varying the chemical potential (μ_c) of graphene material. From Figure 2, we can note that the frequency range is chosen from 0 to 10 THz along x-axis, and the percent level of absorption for different chemical potentials of graphene material is chosen along the y-axis. From the graph, it is a fact that a maximum percent level of absorption achieved at chemical potential is equal to 0.9 eV, which is indicated by a red colored curve. From Figure 3, we can note that it is a contour representation of Figure 2. Here, the frequency range is chosen from 0 to 10 THz along the x-axis, and the chemical potential of graphene material is chosen from 0.4 eV to 0.9 eV along the y-axis. From Figure 3, it is noteworthy that whenever the chemical potential is equal to 0.9 eV, the unit cell structure achieves a maximum percent level of absorption ($> 90\%$), as indicated by the red color. The unit cell structure also resonates at three separate absorption peak frequencies of 2.91, 8.1, and 9.61 THz, with absorption bandwidth ranges of (2.66 THz to 3.12 THz), (7.71 THz–8.47 THz), and (9.57 THz–9.63 THz), respectively. The obtained percent levels of absorptions at the absorption peak frequencies of 2.91, 8.1, and 9.61 THz are 96.4%, 98.5%, and 99.71%, respectively.

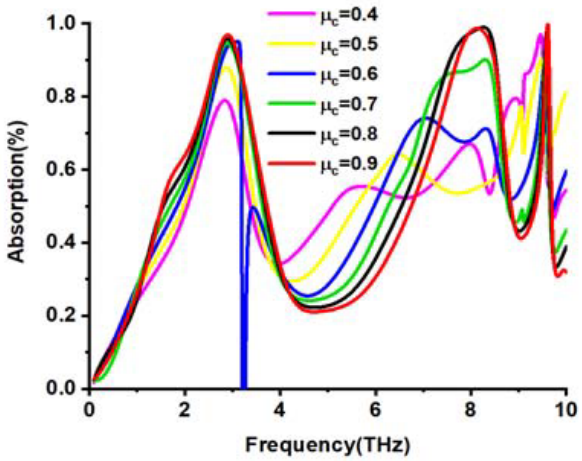

Figure 2. Absorption spectra for variation of different chemical potentials (μ_c).

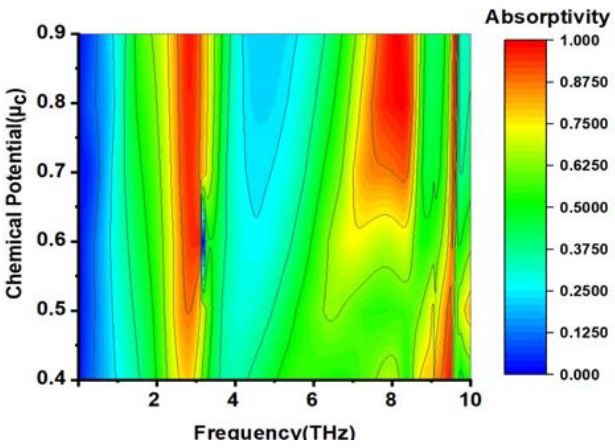

Figure 3. Contour plot for different chemical potentials.

The variation of percent level of absorption for different incident angles (θ), under TE and TM modes, is shown in Figure 4. From Figure 4(a), we can note that for both TE and TM polarizations, the frequency is taken along the x-axis, which is varied from 0.1 to 10 THz, and the incidence angle (θ) of the EM wave is taken along the vertical axis, which is varied from 0 to 90 degrees. Figure 4(a) shows a contour plot by doing a parametric analysis for the incidence angle (θ) under TE mode. From Figure 4(a), it can be noticed that for the first absorption band, a constant bandwidth of 0.46 THz is achieved up to a 55-degree incident angle. Around a 60-degree incident angle, the percent level of absorption indicated with red color has vanished. For the second absorption band, a constant bandwidth of 0.76 THz is achieved up to a 65-degree incident angle. Around a 70-degree incident angle, the percent level of absorption has vanished. For the third frequency band, except at a 0-degree incident angle, for the remaining incident angles, there is no absorption. Figure 4(b) shows a contour plot by doing

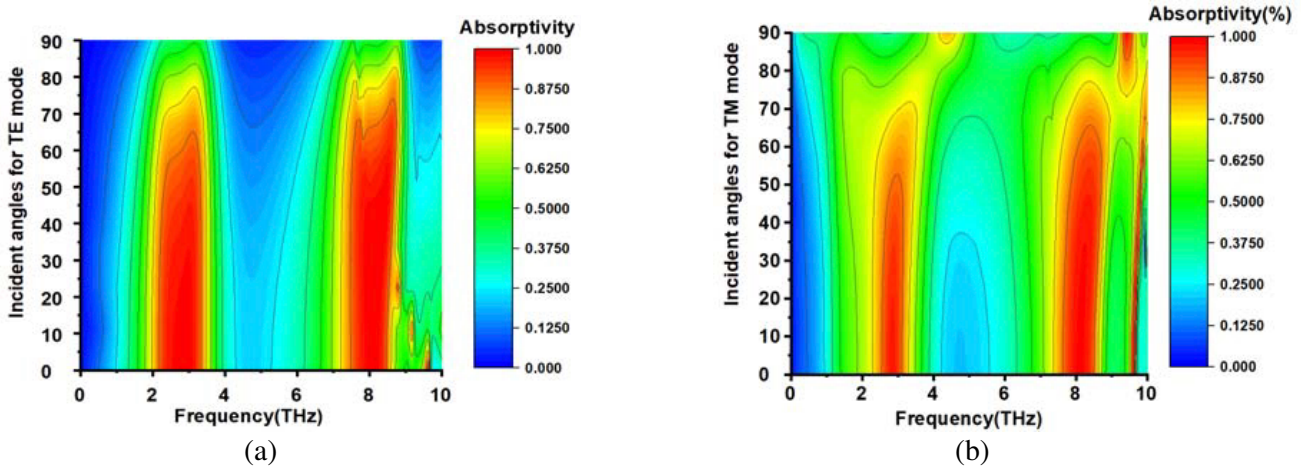

Figure 4. At chemical potential $(\mu_c) = 0.9\,\text{eV}$, the proposed structure's absorption contour map as a function of frequency and different oblique incidence angles (θ) for (a) TE mode and (b) TM mode.

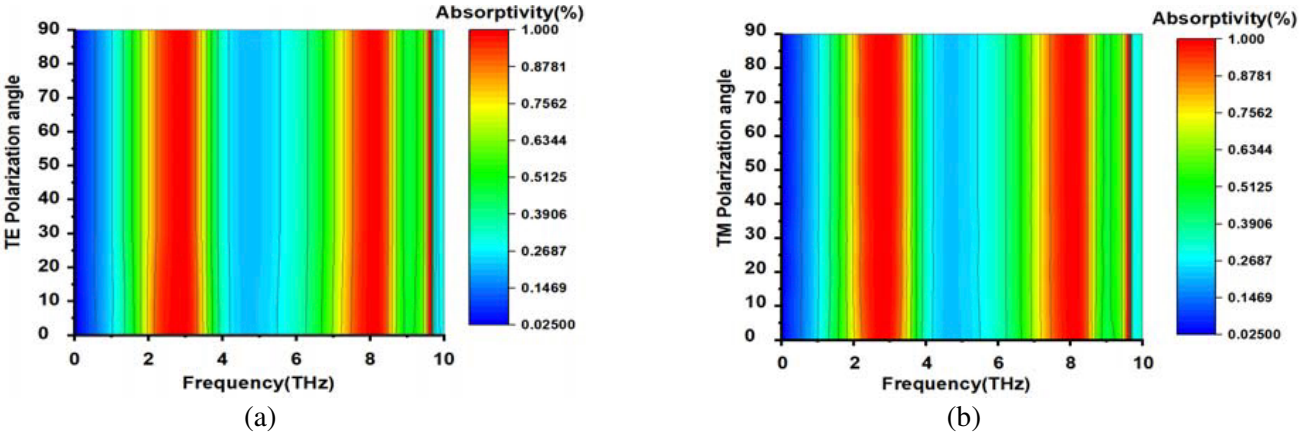

Figure 5. At chemical potential $(\mu_c) = 0.9\,\text{eV}$, the proposed structure's absorption contour map as a function of frequency and different polarization angles (ϕ) for (a) TE mode and (b) TM mode.

a parametric analysis for the incidence angle (θ) under TM mode. from Figure 4(b), it can be noted that for the first absorption band, a constant absorption bandwidth of 0.35 THz is achieved up to a 45-degree incident angle, and around a 50-degree incident angle, the percent level of absorption has vanished. For the second absorption band, a constant bandwidth of 0.76 THz is achieved up to a 60-degree incident angle. Around a 65-degree incident angle, the percent level of absorption vanished, and for the third absorption band, a constant bandwidth of 0.06 THz is achieved up to a 60-degree incident angle. Around a 65-degree incident angle, the percent level of absorption has vanished. The influence of different polarization angles (ϕ) for both TE and TM modes is shown in Figure 5. From Figure 5, we can note that the frequency is taken along the x-axis, which is varied from 0.1 to 10 THz, and the polarization angle (ϕ) of the EM wave is taken along the vertical axis, which is varied from 0 to 90 degrees. Either for TE or TM modes, constant absorption bandwidth is achieved irrespective of any polarization angle.

Figure 6 represents a contour plot for different dielectric thickness values. From Figure 6, we can note that the frequency range is chosen from 0.1 to 10 THz along the x-axis, and the thickness of dielectric material is chosen along the y-axis. A good amount of absorption indicated with red color can be achieved for a silicon dielectric material thickness of 9 micrometers, and at this dielectric thickness, the proposed unit cell resonates at three bands.

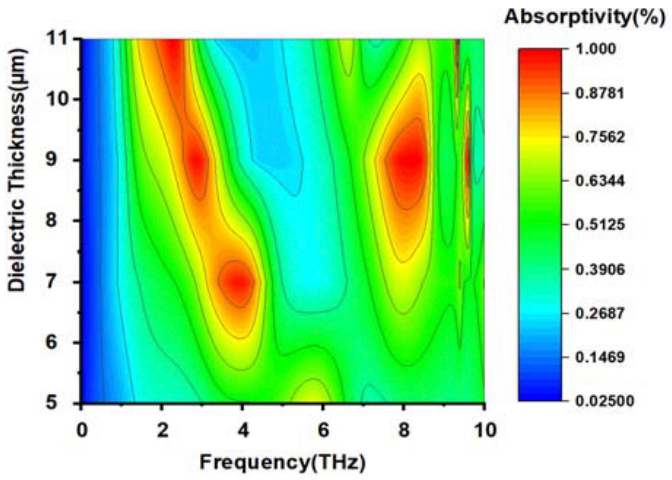

Figure 6. Contour map for the variation of dielectric thickness.

4.1. *E* and *H*-Field Analysis

The structure validation can be done by field distribution analysis like E, H, and surface current. The proposed structure operates at three absorption frequencies of 2.91 THz, 8.1 THz, and 9.61 THz.

Figure 7 and Figure 8 show the electric and magnetic field distributions at three resonant frequencies. From Figure 7(a), we can note that a maximum field intensity is formed corresponding to 2.91 THz frequency on the inner circle of the structure. From Figure 7(b), we can notice that a good amount of electric field intensity is formed corresponding to 8.1 THz frequency between inner and outer circular typed SRRs, and for the 9.61 THz frequency, a maximum amount of intensity is formed on outer circular type SRR and square type SRR. From Figure 8(a), we can notice that the magnetic field corresponds to 2.91 THz frequency forming along the horizontal direction on inner circular type

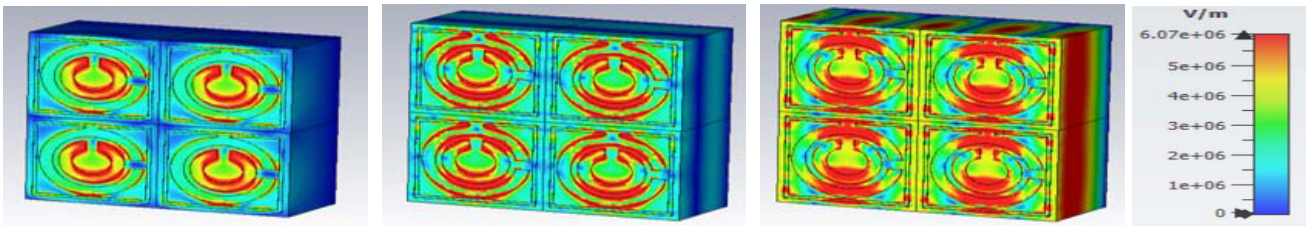

(a) (b) (c)

Figure 7. *E*-field distributions of the unit cell at (a) 2.91, (b) 8.1 and (c) 9.61 THz frequencies.

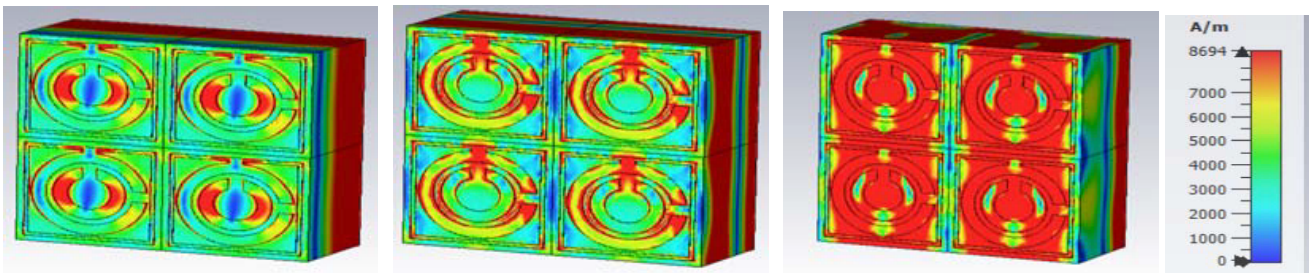

(a) (b) (c)

Figure 8. *H*-field distributions of the unit cell at (a) 2.91, (b) 8.1 and (c) 9.61 THz frequencies.

SRR. Similarly, the magnetic field is formed along the vertical direction for 8.1 THz frequency, and at 9.61 THz frequency, the field is spread on the total conductive patch of the structure. With Figure 7 and Figure 8 we can decide that E- and H-fields are formed in opposite directions as they are perpendicular to each other.

4.2. Validation of the Proposed Unit Cell with a Equivalent Circuit Approach

The validation of the structure through an equivalent circuit diagram is important to justifying the structure's performance. As shown in Figure 1, the unit cell contains a square-typed ring and two circular-typed SRRs. Each SRR is represented by a parallel LC combination. From Figure 9, we can notice that the inner circular type SRR is represented by $L8$ and $C2$, the outer circular type SRR represented by $L2$ and $C1$, and the gap between inner and outer SRRs represented by capacitors $C4$ and $C5$. The outer square type ring is two inductors as it is attached to a strip which is indicated by inductor $L7$, and the gap between the square type ring and outer circular type ring is represented by a capacitor $C6$. The dielectric material of the structure is set to 50 ohms, and finally, it is terminated by ground as the bottom of the structure contains a perfect conducting medium like gold. While doing the simulation, an impedance of 50 ohms is attached to the input of the circuit diagram to provide impedance matching, and in the S-parameter simulation setup, start and stop frequencies are chosen as 0.1 THz to 10 THz frequencies with a step size of 100 GHz.

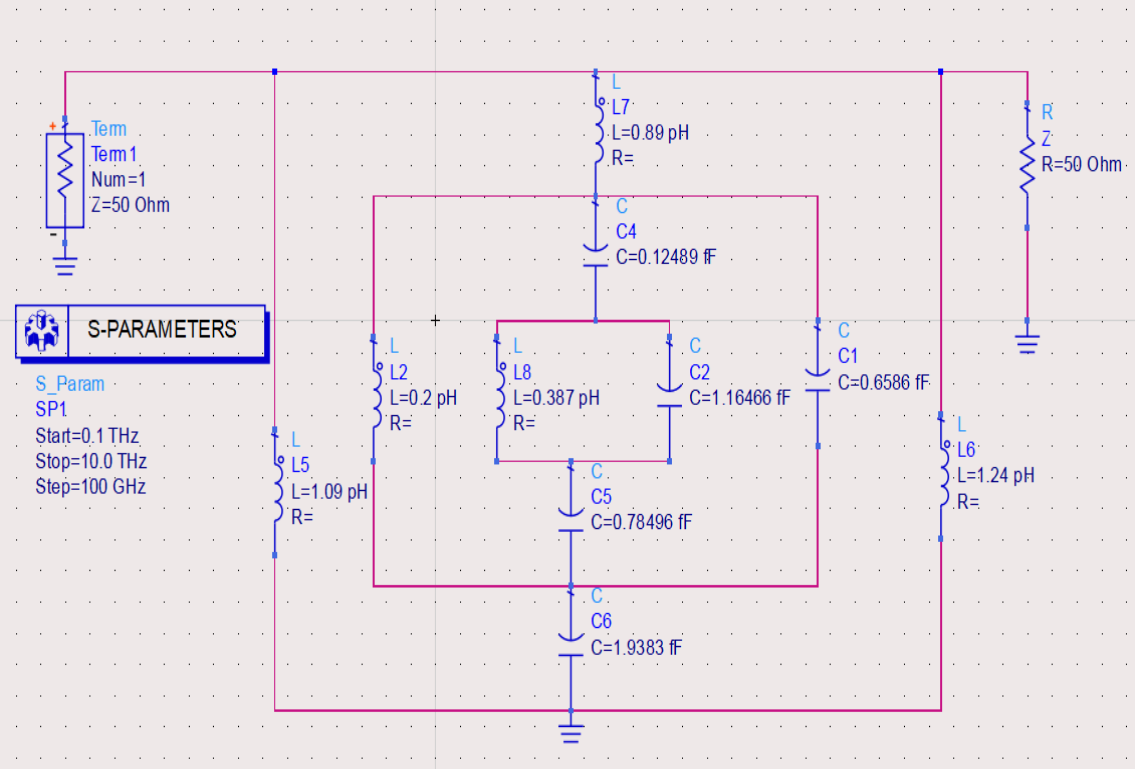

Figure 9. Equivalent lumped circuit model for the proposed unit cell in ADS tool.

From Figure 10, we can note that the red color curve indicates the absorption plot for the Advanced Design System (ADS) tool, and the black color indicates the absorption plot for the Computer Simulation Technology (CST) tool. From Figure 10, we can conclude that the responses from CST and ADS tools are matched concerning absorption percentage and the number of bands. Table 2 indicates present research work with existing state of art. According to Table 2, it can be noted that the proposed

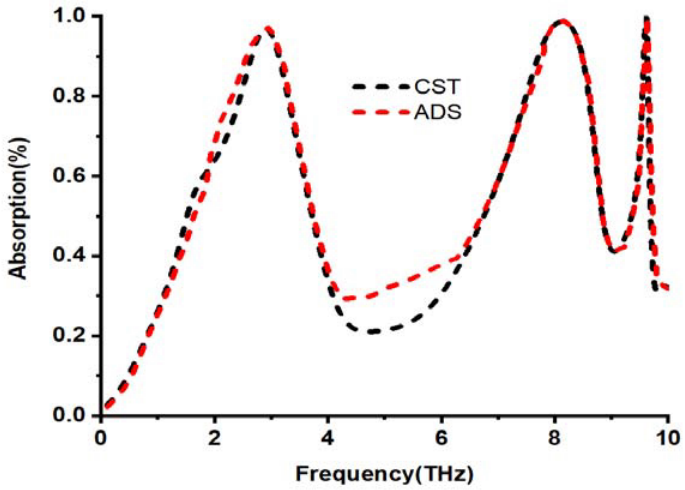

Figure 10. Comparison of absorption for the unit cell structure with ADS and CST tools.

Table 2. Comparision of present work with existing research.

Reference	No. of dielectric materials	Polarization stability	Materials used	Absorption peak frequencies (THz)	Percent level of absorption for the corresponding resonant peaks (%)
[10]	single	-	Polymide, Aluminium, Graphene	0.68 and 2.02 2.04 and 2.58 0.68 and 2.02	58 and 66 58.6 and 91.9 78.1 and 68.6
[11]	two	Up to 90°	VO2, Au, graphene	6.4, 7.32, 8.49, 9.78	95.2, 97, 89.1, 73.3
[14]	two	-	Graphene, Gold, Sio_2	1 to 2	92
[16]	single	Up to 60°	Polymide, graphene, gold	0.65, 1, 1.33, 1.45, 1.74, 0.95	90, 78, 98, 99, 91, 71
[17]	single	-	Topas, graphene, gold	1.8, 2.62, 3.72	88, 89, 92
[18]	Two	NO	graphene, Sio_2, Au	1.29, 3.32, 3.85, 4.56	95.4, 99.9, 89.4, 98.9
[19]	single	YES	Aluminium, PET	0.337, 0.496, 0.718	99.5, 86.4, 98.4
[20]	single	Up to 90°	Al, PET	0.479, 1.04, 1.15	98, 91, 98
This work	single	Up to 90°	Silicon, Au, Graphene	2.91, 8.1, 9.61	96.4, 98.5, 99.71

absorber produces triple bands with absorption percentages more than 96 percentage. Compared to all the research works listed in Table 2, the proposed structure is a compact and straightforward structure, which provides a polarization-insensitive ability up to 90 degrees with a percent level of absorption greater than 90.

5. CONCLUSION

We propose a graphene-based triband absorber made up of a split rings-based graphene layer and a bottom reflector made up of gold isolated by a Silicon substrate. Polarization angle-independent broadband absorption is achieved through continuous plasmon resonances supported by graphene material. The proposed unit cell structure resonates at three different absorption peak frequencies of 2.91 THz, 8.1 THz, and 9.61 THz with absorption percentages of 96.4, 98.5, and 99.71 respectively. At a chemical potential of 0.9 eV, the percent level of absorption ($> 90\%$) can be obtained for (2.66 THz to 3.12 THz), (7.71 THz–8.47 THz), and (9.57 THz–9.63 THz) frequency bands, respectively. The proposed unit cell is represented with an equivalent lumped circuit model for validating the structure performance. Hence, it can be concluded that the proposed structure is a straightforward configuration with three layers and achieves tri-bands with a percent level of absorption greater than 90 percent and absorption bandwidth as constant irrespective of any polarization angle.

REFERENCES

1. Roy, S. and K. Debnath, "Electromechanically tunable graphene-based terahertz metasurface," *Optics Communications*, Vol. 534, 129319, 2023.
2. Cornejo, H. S., L. De Los Santos Valladares, V. S. Kamboj, A. Bustamante Dominguez, J. C. González, A. M. Osorio Anaya, N. O. Moreno, et al., "Texture and terahertz analysis of $YBa_2Cu_3O_7$ grown onto $LaAlO_3$ by the chemical solution deposition," *Heat Treatment*, Vol. 3, No. 1, 1–8, 2022.
3. Shur, M. S., "Terahertz plasmonic technology," *IEEE Sensors Journal*, Vol. 21, No. 11, 12752–12763, 2020.
4. Latha, A. M., S. Unnikrishnakurup, A. Jain, M. K. Pathra, and K. Balasubramaniam, "Material characterization and thickness measurement of iron particle reinforced polyurethane multi-layer coating for aircraft stealth applications using THz — Time domain spectroscopy," *Journal of Infrared, Millimeter, and Terahertz Waves*, Vol. 43, Nos. 7–8, 582–597, 2022.
5. Patel, S. K., J. Surve, and J. Parmar, "Detection of cancer with graphene metasurface-based highly efficient sensors," *Diamond and Related Materials*, Vol. 129, 109367, 2022.
6. Strag, M. and W. Swiderski, "Defect detection in aramid fiber-reinforced composites via terahertz radiation," *Journal of Nondestructive Evaluation*, Vol. 42, No. 1, 2023.
7. Ergün, S. and S. Sönmez, "Terahertz technology for military applications," *Journal of Management and Information Science*, Vol. 3, No. 1, 13–16, 2015.
8. Xu, C., Z. Ren, J. Wei, and C. Lee, "Reconfigurable terahertz metamaterials: From fundamental principles to advanced 6G applications," *Iscience*, Vol. 25, No. 2, 103799, 2022.
9. Sabah, C., B. Mulla, H. Altan, and L. Ozyuzer, "Cross-like terahertz metamaterial absorber for sensing applications," *Pramana*, Vol. 91, 1–7, 2018.
10. Zhou, S., K. Bi, Q. Li, L. Mei, Y. Niu, W. Fu, S. Han, et al., "Patterned graphene-based metamaterials for terahertz wave absorption," *Coatings*, Vol. 13, No. 1, 59, 2023.
11. Li, J., Y. Liu, Y. Chen, W. Chen, H. Guo, Q. Wu, and M. Li, "Tunable broadband-narrowband and dual-broadband terahertz absorber based on a hybrid metamaterial vanadium dioxide and graphene," *Micromachines*, Vol. 14, No. 1, 201, 2023.
12. Zhang, Z., Q. Sun, Y. Fan, Z. Zhu, J. Zhang, X. Yuan, and C. Guo, "Low-threshold and high-extinction-ratio optical bistability within a graphene-based perfect absorber," *Nanomaterials*, Vol. 13, No. 3, 389, 2023.
13. Upender, P. and A. Kumar, "THz dielectric metamaterial sensor with high Q for biosensing applications," *IEEE Sensors Journal*, 2023.
14. Beheshti Asl, A., D. Pourkhalil, A. Rostami, and H. Mirtaghioglu, "A perfect electrically tunable graphene-based metamaterial absorber," *Journal of Computational Electronics*, Vol. 20, 864–872, 2021.

15. Yi, Z., J. Chen, C. Cen, X. Chen, Z. Zhou, Y. Tang, X. Ye, S. Xiao, W. Luo, and P. Wu, "Tunable graphene-based plasmonic perfect metamaterial absorber in the THz region," *Micromachines*, Vol. 10, No. 3, 194, 2019.
16. Ashvanth, B., B. Partibane, and G. Idayachandran, "Designing miniaturized metamaterial absorber with tunable multiband characteristics for THz applications," *Bulletin of Materials Science*, Vol. 44, 1–8, 2021.
17. Xu, K.-D., Y. Cai, X. Cao, Y. Guo, Y. Zhang, and Q. Chen, "Multiband terahertz absorbers using T-shaped slot-patterned graphene and its complementary structure," *JOSA B*, Vol. 37, No. 10, 3034–3040, 2020.
18. Jain, P., K. Prakash, G. M. Khanal, N. Sardana, S. Kumar, N. Gupta, and A. K. Singh, "Quad-band polarization sensitive terahertz metamaterial absorber using Gemini-shaped structure," *Results in Optics*, Vol. 8, 100254, 2022.
19. Wang, J., T. Lang, Z. Hong, M. Xiao, and J. Yu, "Design and fabrication of a triple-band terahertz metamaterial absorber," *Nanomaterials*, Vol. 11, No. 5, 1110, 2021.
20. Abdulkarim, Y. I., M. Xiao, H. N. Awl, F. F. Muhammadsharif, T. Lang, S. R. Saeed, F. Alkurt, M. Bakır, M. Karaaslan, and J. Dong, "Simulation and lithographic fabrication of a triple band terahertz metamaterial absorber coated on flexible polyethylene terephthalate substrate," *Optical Materials Express*, Vol. 12, No. 1, 338–359, 2022.
21. Li, H. and J. Yu, "Active dual-tunable broadband absorber based on a hybrid graphene-vanadium dioxide metamaterial," *OSA Continuum*, Vol. 3, No. 7, 2143–2155, Aug. 15, 2020.
22. Nickpay, M. R., M. Danaie, and A. Shahzadi, "A wideband and polarization-insensitive graphene-based metamaterial absorber," *Superlattices and Microstructures*, Vol. 150, 106786, Feb. 1, 2021.
23. Zhuang, S., X. Li, T. Yang, L. Sun, O. Kosareva, C. Gong, and W. Liu, "Graphene-based absorption — Transmission multi-functional tunable THz metamaterials," *Micromachines*, Vol. 13, No. 7, 1239, Aug. 1, 2022.